ACS Catalysis

Research Article

pubs.acs.org/acscatalysis

ALD of Ultrathin Ternary Oxide Electrocatalysts for Water Splitting

Katie L. Pickrahn, Aaron Garg, and Stacey F. Bent*

Department of Chemical Engineering, Stanford University, 443 Via Ortega, Stanford, California 94305-5025, United States

Supporting Information

ABSTRACT: Semiconducting oxides, particularly mixtures of different transition-metal oxides, are promising materials for oxygen evolution reaction (OER) catalysts. Assessment of these materials is often complicated by inadequate dispersion of the materials, charge transport limitations, and lack of surface area characterization. Thin films deposited by atomic layer deposition (ALD) present an excellent way to overcome these issues. Here, we present the first work using ALD to investigate ternary oxide electrocatalysts, specifically with the Ti−Mn ternary oxide system. Thin-film mixtures of between 1.4 and 2.8 nm in thickness are successfully synthesized by ALD and show a high degree of mixing. At compositions between ∼10 and 70% Mn: (Mn+Ti), there is a reduction in ALD growth rate relative to the growth rates of the binary constituents. Moreover, we observe a shift in the chemical binding energies of both Mn and Ti over this composition range. An elevation in the activity of Mn active sites for OER is observed with increasing MnO_x content in TiO_2, increasing the turnover frequency (TOF) by approximately an order of magnitude. These results are consistent with previous DFT calculations. We also explore the effect of film thickness of the ternary metal oxide on catalytic activity, highlighting how ALD allows for charge transport limitations to be minimized.

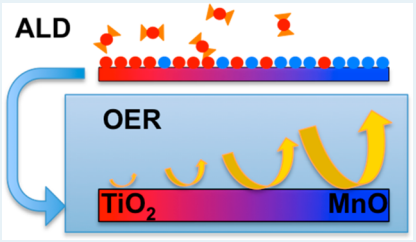

KEYWORDS: *ALD, electrocatalysts, ternary oxide, MnO_x, TiO_2, oxygen evolution reaction*

I. INTRODUCTION

Catalysts for the oxygen evolution reaction (OER) are critical in many energy-transforming technologies, including solar fuel generation, metal−air batteries, and regenerative fuel cells.[1−5] Catalysts must not only efficiently catalyze the reaction but also be stable under the harsh oxidizing conditions of OER and preferably be of low cost. Metal oxides are particularly promising candidates for OER catalysts. Precious metal oxides including IrO_x and RuO_x[6,7] along with earth-abundant metal oxides such as MnO_x, CoO_x, and NiO_x have been identified as promising choices. Unfortunately, the four-electron OER process in which water is oxidized to oxygen remains one of the main sources of overpotential for these technologies, and advances in earth-abundant OER catalysts are critical for improving their economic feasibility. Mixtures of semiconducting oxide materials have shown much promise as OER catalysts, although these materials are often difficult to characterize.[8−12]

Thin films provide an excellent model system to test and compare mixtures of semiconducting oxide materials. First, thin films can assist in decoupling the effects of charge transport and catalytic activity of a surface, which is of great importance in electrochemical testing of semiconducting thin films.[13,14] Second, the use of thin films allows for less variation in the surface roughness and decreases mass transport losses, enabling better characterization of the active surface area.[15−17] Such effects are particularly important in metal oxides, where it is difficult to determine the number of active sites.[10] Third, thin films cannot support a large depletion region, making the activity less dependent on carrier concentration and interfacial contact problems.[11] These thin films can then be applied to highly structured substrates to achieve high geometric or volumetric activity.

Atomic layer deposition (ALD) is an excellent method of depositing high quality, uniform thin films. ALD is a vapor phase deposition technique consisting of a series of self-limited, saturated half-reactions.[18−20] Substrates are sequentially exposed to reactants or counter-reactants until a film of the desired thickness is reached. ALD is gaining increasing attention in the catalysis field. It has been used to deposit catalytic metallic thin films such as Pt,[21] Ir,[22] and Pd[23] along with metal oxide films such as MnO_x,[24] VO_x,[25] and CoO_x,[26] often taking advantage of ALD's ability to uniformly coat high-surface-area supports. While metal and binary oxides are relatively straightforward to synthesize by ALD, ternary oxides are often much more complicated to deposit.[27−29] The chemistry of the ligands and counter-reactants must be chosen to be compatible, and factors such as etching, self-catalysis of ALD reactions, and nucleation can affect deposition. Nevertheless, ternary oxide films deposited by ALD have already been used in a variety of applications, including tribology coatings,[30] high-k dielectrics,[31] transparent conducting oxides,[32,33] and buffer layers.[34] However, despite the many interesting applications of ternary oxides as electrochemical catalysts, including for OER, to our knowledge there have been no previous reports of ternary oxide electrocatalysts deposited by ALD. In this work, we study thin films of mixed Mn and Ti oxides as OER catalysts.

We have previously shown that ALD-MnO_x—an earth-abundant, nontoxic, bioinspired OER catalyst—is as active as some of the best MnO_x catalysts in the literature.[24] Like most

Received: October 7, 2014
Revised: December 30, 2014
Published: January 26, 2015

DOI: 10.1021/cs501532b
ACS Catal. 2015, 5, 1609−1616

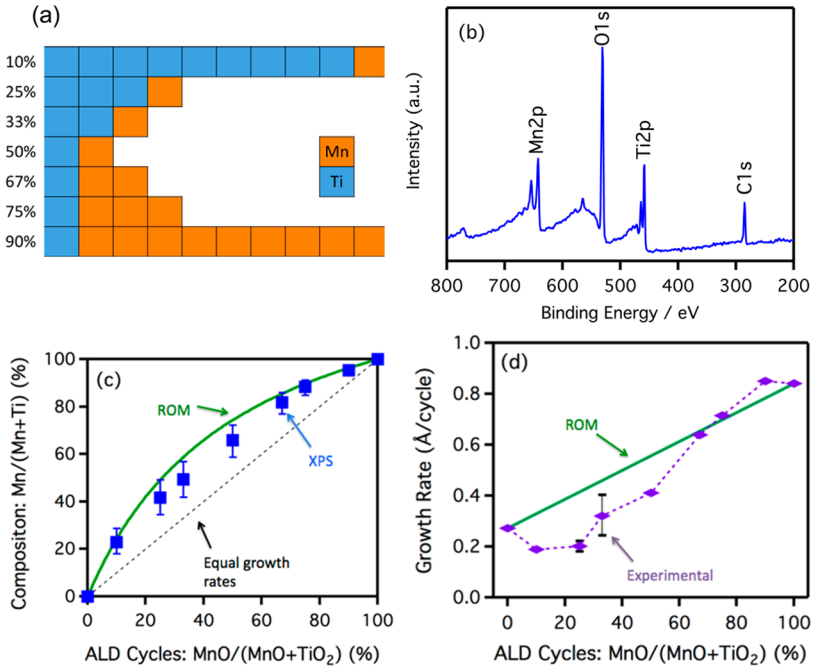

Figure 1. Thin films of mixtures of Ti and Mn oxides were grown by ALD using the supercycle sequences shown in (a). Each square consists of a metal-precursor pulse and a water pulse, and the macrocycles always end with MnO. These ALD processes produce films containing both Mn and Ti, as shown by a XPS survey scan (b) of a 33% MnO ALD cycle film. (c) Experimental composition from XPS of the thin films closely follows the expected composition from the weighted average of the growth rates (rule of mixtures, ROM). Error bars reflect the error associated with the XPS measurement. It appears the films are slightly Mn deficient. (d) Theoretical growth rates from the ROM are compared to the experimental growth rates. A large suppression in the growth is observed for films between ~10 and 70% MnO by ALD cycle. Error bars from three unique ALD runs at 25% and 33% indicate the reproducibility of these results.

explored transition-metal oxides, its activity for the OER can be related to a single descriptor, $\Delta G_{O^*} - \Delta G_{OH^*}$, which captures how strongly the intermediates bind to the surface.[35] From DFT calculations, it appears that O* binds too strongly to the manganese oxides.[35] TiO_2 is commonly found in OER catalysts such as dimensionally stable anodes (DSAs) due to its high stability, although it binds too weakly to O* to act as a catalytically active site.[36] In metallic systems, the strength of the binding may be altered by alloying two metals, one of which binds the intermediates too strongly and one of which binds too weakly, to alter the binding of the catalyst and create more active catalysts.[37,38] Mixing metal oxides has been proven to create more active catalysts as well.[11,39] DFT calculations have indicated that mixing TiO_2 and transition-metal oxides can alter the binding of the catalytic intermediaries to the metal ions and may produce highly active catalysts.[40] A high level of mixing would be needed to achieve these effects, and ALD has the potential to achieve this mixing along with a fine control over film thickness.

In this work, we deposit thin films of Mn and Ti oxides over the full span of their compositions by ALD. First, we show that these thin films can be synthesized and correlate measured growth rate with the expected growth rate from the rule of mixtures, which is a weighted average of the individual binary oxide growth rates. For low levels of Mn, a significantly decreased growth rate is found. However, the film composition, as determined by XPS, is close to the expected value over the entire span of compositions. Shifts in the Ti-$2p_{3/2}$ and Mn-$2p_{3/2}$ XPS peaks with composition suggest intimate mixing within the film. Second, we test the effect of composition on the $MnTi_xO_y$ catalytic activity for OER. The activity of the films monotonically increases with increasing content of Mn. The presence of Ti appears to suppress the overall activity of the Mn. Third, we show the importance of using thin films to characterize these mixed-metal oxide systems and illustrate how charge transport limitations can mask the activity of a film.

II. METHODS

A careful choice of precursors and ALD conditions is necessary for the growth of a ternary oxide system. Bis(ethylcyclopentadienyl)manganese ($Mn(EtCp)_2$ Strem Chemicals), titanium tetraisopropoxide (TTIP, Aldrich), and water were used as the Mn source, Ti source, and O source, respectively. The saturation conditions for the binary oxide components were selected from previous reports[24,41−43] and reevaluated throughout sample preparation. The precursors for these systems were chosen to have compatible ALD windows. Both TTIP and $Mn(EtCp)_2$ use water as the counter reactant. The ALD window is reported to be between ~190 and 260 °C for the formation of TiO_2[42,43] and between 100 and 300 °C for the formation of MnO.[41] A stage temperature of 200 °C, falling within both systems' ALD windows, was selected. The chemistry of the reactants was also chosen to avoid formation of more stable non-oxide byproducts. For example, the use of $TiCl_4$ as the Ti source leads to the formation of $MnCl_2$, which interferes with the desired ALD behavior.

ALD was performed in a custom-built, hot-wall ALD reactor complete with five ports for precursors. Films were deposited at 200 °C with a continuous N_2 flow rate of 10 sccm. Silicon (100) wafers (WRS Materials) used as witness wafers to measure ALD film thickness were cleaned with O_3 for 15 min immediately prior to use. ALD samples for catalytic testing were deposited on FTO (TEC 8, Hartford Glass). The FTO was cleaned prior to ALD by sonicating in acetone for 30 min,

DOI: 10.1021/cs501532b
ACS Catal. 2015, 5, 1609−1616

followed by sonication in DI H_2O for 30 min. Film composition was confirmed by XPS to be the same between the FTO and the Si wafers. The deposition consisted of a 2 s pulse of the metal precursor, a 50 s purge, a 2 s pulse of water, and a 65 s purge, repeated to obtain the desired thickness. Sample deposition was designed to create the highest amount of material mixing possible by using the lowest ratio of cycles for the desired composition. For example, a 25% Mn:(Mn+Ti) sample (by cycle number) consisted of 20 supercycles comprised of 3 TTIP/H_2O and 1 $Mn(EtCp)_2/H_2O$ individual cycles to get a film ∼1.5 nm thick. The last cycle consisted of $Mn(EtCp)_2/H_2O$ for all samples except for the 0% Mn:(Mn+Ti) film to keep the surfaces consistent. Samples were removed from the reactor at 200 °C.

Sample thickness was characterized on Si wafers using ellipsometry (Woolam α-SE). Measurements taken at 65, 70, and 75° were used in the fitting. Sample thickness was modeled using both a model optimized for TiO_2 and a model optimized for MnO. For thin samples (<4 nm), both models gave a thickness within 1 Å of one another. Models for thicker samples (4−35 nm) had less than an 8% difference in thickness, and the reported thickness was estimated from the model closest to its composition.

XPS measurements were taken on a PHI VersaProbe Scanning XPS Microprobe with Al Kα radiation of 1486 eV. To determine the composition of the film, survey scans were taken. The ratio of the areas of the Mn $2p_{3/2}$ and Ti 2p peaks was used to find the percent composition of the metal ions of these films. High-resolution scans of the Ti 2p and Mn $2p_{3/2}$ regions were also completed to examine shifts in the binding energy.

Catalytic OER testing was performed in a home-built Teflon compression cell. The electrolyte was 0.1 M KOH prepared with Milli-Q H_2O (18.2 M Ω) and was purged continuously through a glass sparger with Ar. A coiled Pt wire served as the counterelectrode, and a Ag|AgCl reference electrode was used. The potentials were controlled using a Bio-Logic SP-200 potentiostat. An area of 0.5 cm^2 was exposed to the electrolyte, and conductive Cu tape was used to make contact with the FTO. Samples were purged with Ar for 5 min. The samples were then polarized between 1.1 and 1.9 V_{RHE} at a scan rate of 20 mV/s for 11 sweeps. The resistance of the electrolyte was accounted for by *iR* compensation at 85%. A lower bound for the TOF was estimated by assuming all Mn atoms in the film were catalytically active and assuming a bulk MnO crystal structure for the thin films.

Redox experiments to probe the conductivity of the sample were completed in a setup similar to that for the OER testing. An electrolyte consisting of 0.1 M $K_4Fe(CN)_6$ (Sigma-Aldrich), 0.1 mM $K_3Fe(CN)_6$ (Sigma-Aldrich), and 0.1 M KOH was used, and the electrolyte was continuously purged with Ar. The potential was scanned between 0.66 and 1.76 V_{RHE} at a scan rate of 20 mV/s.

III. RESULTS AND DISCUSSION

The films were grown by the ALD process described in the Methods section using the smallest number of subcycles to achieve each desired composition, as shown in Figure 1a. This was done to maximize mixing and promote the formation of Mn−O−Ti bonds. XPS survey scans were taken of each sample, as illustrated by the spectrum for a 33% Mn:(Mn+Ti) (by cycle number) film shown in Figure 1b. The XPS results demonstrate that both Ti and Mn are present in the mixed films in all cycle ratios from 10 to 90% Mn:(Mn+Ti). Under the deposition conditions used, ALD of pure MnO has a growth rate of 0.8 Å/cycle, while ALD of TiO_2 has a growth rate of 0.3 Å/cycle. Thus, we do not expect the composition of the films to be proportional to the number of cycles. Instead, the expected concentration of metal ions can be estimated by the rule of mixtures (ROM):[28]

$$\%\ \mathrm{Mn}_{\mathrm{ROM}} = \frac{\alpha_{\mathrm{Mn}}\beta_{\mathrm{Mn}}}{\alpha_{\mathrm{Mn}}\beta_{\mathrm{Mn}} + \alpha_{\mathrm{Ti}}(1-\beta_{\mathrm{Mn}})} \times 100$$

where α_x is the growth rate of metal oxide x and β_x is the fraction of cycles of metal oxide x. The saturated growth rate for each binary material, α_x, is measured using ellipsometry and is consistent with our results reported elsewhere,[14,24] and β_x is determined by the ALD procedure used to make each composition shown in Figure 1a. The green line in Figure 1c maps the expected composition in atom % Mn of the metal ions (i.e., not including oxygen) from the ROM. These values are compared to experimental results obtained by XPS of Mn and Ti in the mixtures for films between 1.4 and 2.8 nm in thickness. Error bars are estimated by including a 20% error in the measurement of each element, approximating the error in the XPS measurement. The experimental values and expected values from the ROM are in good agreement, although the amount of Mn measured by XPS consistently appears to be slightly lower than the expected ROM. Likely the film growth rate changes when growing on ternary oxides in comparison to the binary components.

To investigate this effect, we measured the changes in the growth rate of the ternary oxides in comparison to the binary oxide components. The expected growth rate (GR_{ROM}) assuming the materials grow independently from one another can be found from the ROM:

$$\mathrm{GR}_{\mathrm{ROM}} = [\alpha_{\mathrm{Mn}}\beta_{\mathrm{Mn}} + \alpha_{\mathrm{Ti}}(1-\beta_{\mathrm{Mn}})]$$

In actuality, the growth rate is likely to change when one material is deposited onto a dissimilar material. We calculate the experimental growth rate from the measured thickness, d_{exptl} and the number of cycles, as follows:

$$\mathrm{GR}_{\mathrm{exptl}} = \frac{d_{\mathrm{exptl}}}{A+B}$$

where A and B are the total number of Mn and Ti ALD cycles. In Figure 1d, GR_{ROM} and GR_{exptl} are plotted versus composition for films between 1.4 and 2.8 nm. We find that, for these thin films, there is a large suppression in the expected growth rate when the Mn concentration is between ∼10 and 60% Mn:(Mn+Ti) (by cycle number). For example, a film containing 42 atom % Mn:(Mn+Ti) by XPS (25% by cycle number) that has a GR_{ROM} value of 0.41 Å/cycle only has a GR_{exptl} value of 0.19 Å/cycle, representing a decrease in the average growth rate of over 50% (5.6 nm film versus a 2.6 nm film). A minimum of three ALD runs performed for thin 25% and 33% Mn:(Mn+Ti) (by cycle number) films confirms the repeatability of the low growth rates for films with low concentrations of Mn, as shown by the error bars in Figure 1d. Films with a higher concentration of Mn may have a slight increase in the observed growth rate in comparison to the expected value.

We hypothesize that the changes in the ALD growth rate may be related to the number of surface reaction sites produced by a precursor landing on the surface. The Mn precursor,

DOI: 10.1021/cs501532b
ACS Catal. 2015, 5, 1609−1616

$Mn(EtCp)_2$, and Ti precursor, TTIP, have two and four ligands, respectively, which can exchange with surface groups. The number of ligands that react with the surface will control the number of available sites for the next ALD cycle. For example, if TTIP reacts at the MnO-terminated surface via three of its ligands, then the surface reaction site density will decrease, causing a decrease in the growth rate for subsequent cycles and an overall decrease in the growth rate of a mixture. A similar explanation has been suggested by Tanskanen et al. for a ZnO−SnO_2 ALD system grown from diethylzinc (DEZn) and tetrakis(dimethylamido)tin (TDMASn).[29] Analogous to the system studied in this paper, DEZn has two ligands and TDMASn has four ligands. Tanskanen et al. found a decrease in the growth in the ternary ZnO−SnO_2 ALD system in comparison to the constituent binary components that could be accounted for by a thermodynamically favorable three-ligand exchange of TDMASn on a ZnO surface.[29] However, applying this model to our study will require additional understanding of how many ligands TTIP exchanges on a MnO surface. It is possible that other factors, including changes in the reactivity of the individual reaction sites or etching, may come into play.

The effect of the compositional mixing on the binding in the $MnTi_xO_y$ ternary oxides has been investigated by high-resolution XPS scans of the metal ions. The Ti $2p_{3/2}$ core level peak is shown in Figure 2a. A shift of the Ti $2p_{3/2}$ peak to lower binding energy with increasing Mn concentration is observed, going from 459.0 eV for pure TiO_2 to 458.2 eV for a film containing 95 atom % Mn:(Mn+Ti). The value of 459.0 eV is typical for Ti^{4+},[44] and the presence of Mn appears to slightly reduce the average oxidation state of the Ti. The Mn $2p_{3/2}$ peak for different concentrations is plotted in Figure 2b. Due to the broad nature of the Mn $2p_{3/2}$ peak, it is difficult to assign an exact oxidation state from peak position alone, but the lack of a satellite peak for the Mn^{2+} in the samples is consistent with the surface of the MnO oxidizing in air to form a $Mn^{3+/4+}$ mixture.[24] There is also a shift to lower binding energy of ∼1 eV in the Mn $2p_{3/2}$ peak position with increasing Mn concentration. These higher binding energies are associated with a film containing more highly oxidized Mn. The shifts in the binding energy of the Ti $2p_{3/2}$ and Mn $2p_{3/2}$ peaks are consistent with previous reports of doping TiO_2 thin films and are indicative of the formation of Mn−O−Ti bonds.[44,45] These high-resolution scans show that the mixing of Mn and Ti affects the electronic properties of the materials, suggesting good intermixing in the films.

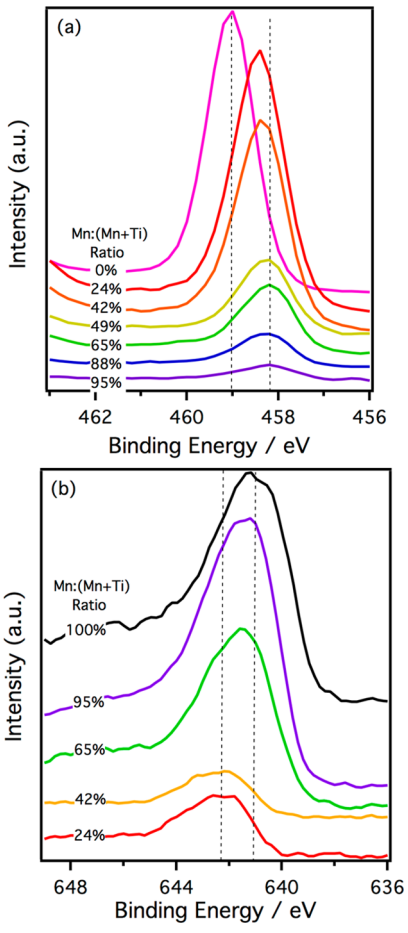

Figure 2. High-resolution XPS scans of the (a) Ti $2p_{3/2}$ and (b) Mn $2p_{3/2}$ regions, revealing shifting chemical states with changing composition. These shifts are indicative of the formation of Mn−O−Ti bonds.

We now look at how the composition affects the catalytic activity of the $MnTi_xO_y$ thin films for OER. The first sweep of a cyclic voltammogram in the anodic direction is plotted in Figure 3a. The sample films are all between 1.4 and 2.8 nm thick (i.e., thin enough to avoid charge transport limitations); thus, we are probing differences in the activity of the surface rather than differences in charge transport. A bare FTO substrate is included for reference. The catalytic activity decreases monotonically with increasing amounts of Ti in the film. It is well-known that the catalytic activity of MnO_x is greater than that of TiO_2 for OER.[14,24] Hence, it can be assumed that the effect is related predominantly to the decreasing amount of MnO_x active sites.

To more clearly quantify the change in activity with composition, we plot in Figure 3b the current density, j, measured at 1.85 V versus the composition ratio determined from XPS. At least three samples were tested for each point, and error bars indicate one standard deviation. If the presence of Ti simply decreased the number of MnO_x active sites, we would expect the current density obtained to follow the stoichiometric current density, j_{stoich}. The j_{stoich} value is calculated by assuming that the current density is proportional to number of Mn and Ti sites in the film:

$$j_{stoich} = j_{Mn}\chi_{Mn} + j_{Ti}\chi_{Ti}$$

where j_x is the current density for a given voltage for a binary oxide of element x and χ_x is the fraction of surface sites of element x. The j_{stoich} values are plotted as the dotted line in Figure 3b. However, instead of matching the j_{stoich}, we observe a suppression in the catalytic activity of the Mn with increasing Ti which is larger than that expected from the stoichiometry. Because the experimental points are based on XPS composition, which considers the bulk of the film rather than simply the surface, there will be a small systematic error toward lower atom % Mn. Namely, since all Mn-containing films were terminated with a MnO ALD cycle, the electrochemically active surface likely contains a greater amount of Mn. Thus, the error would be a shift of the experimentally derived current densities to higher Mn content, further increasing the apparent suppression in the films. The suppression in activity is also clearly observed when plotting current density per mass loading of Mn (Figure S1 in the Supporting Information). The TOF of the Ti−Mn ternary oxides was estimated by assuming all Mn

DOI: 10.1021/cs501532b
ACS Catal. 2015, 5, 1609−1616

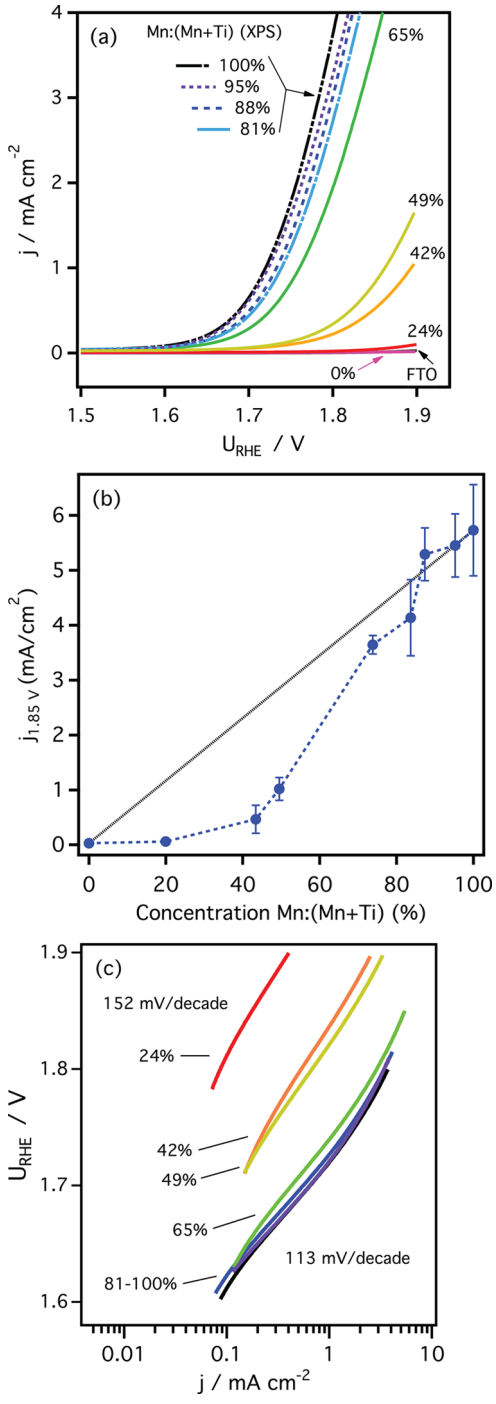

Figure 3. (a) Anodic direction of CV curves for different compositions of Mn−Ti oxide thin films, showing a monotonic drop in activity with increasing level of Ti. (b) Slice of the current density obtained at 1.85 V further revealing the suppression by the Ti of the activity of the Mn. (c) Tafel slopes of the Mn oxide containing thin films revealing decreasing Tafel slope with increasing Mn composition. If the effect were purely due to a decreased number of active sites, we would expect the current density to follow close to the dashed line in (b) and maintain a similar Tafel slope.

atoms in the film are electrochemically accessible. Since all Mn atoms in the film may not be active, this calculation will estimate a lower bound for the TOF; however, because the films are only on the order of 10 layers of atoms thick, we estimate the TOF to be within 1 order of magnitude of the actual value.[11] Using this approximation, we estimate that the TOF increases by approximately 1 order of magnitude from ∼0.2 s^{-1} for a film containing 24 atom % Mn:(Mn+Ti) to ∼4 s^{-1} for pure MnO_x thin films at an overpotential of 0.63 V. This large increase in TOF indicates that there is a suppression in the inherent catalytic activity of MnO_x due to the presence of TiO_2, most evident at low Mn compositions.

Tafel plots provide further information on the kinetics of the catalysts. They were constructed by plotting the *iR*-corrected voltage versus the logarithm of the current density. As seen in Figure 3c, the Tafel slope decreases with increasing Mn composition, going from 152 mV/decade for a film containing 24 atom % Mn:(Mn+Ti) to 113 mV/decade for 100% MnO_x, supporting the hypothesis that the catalytic sites are becoming increasingly active with Mn concentration. Interestingly, films with greater than 80 atom % Mn:(Mn+Ti) (XPS) all have similar Tafel slopes and similar Ti $2p_{3/2}$ or Mn $2p_{3/2}$ binding energies. This suggests that once a composition of 80% Mn:(Mn+Ti) is reached in the oxide thin films, the effect of the TiO_2 is mainly a reduction in the number of electrochemically accessible Mn active sites. The increase in the Tafel slope at higher current densities for the films with high concentrations of Mn is likely related to mass transport losses. Thus, the impact of the Ti appears to be 2-fold: a stoichiometric effect due to the reduction of the number of active sites and an electronic effect that decreases the activity of the individual active sites at low Mn concentrations. The Ti does not appear to have a significant impact on the stability of the Mn-containing catalysts, and all show a decrease in activity over the 11 CV cycles of around 20−70% (see Figure S2 in the Supporting Information).

The apparent suppression of the Mn activity supports the conclusion from the XPS measurements that Ti and Mn are well mixed and form bonds that can affect the electronic state of the metallic ions. An inspection of the volcano plot in ref 35 suggests that although the Ti weakens the binding of O to Mn, it weakens it too much, surpassing the ideal binding energy.[35] Other authors have used DFT to calculate the effects of doping TiO_2 with Mn on the overpotential for OER.[40] They found that in these systems the Mn is more active than Ti atoms and that Mn sites show an overpotential comparable to or slightly higher than that of the undoped MnO_x, both consistent with our results.

Here we propose further explanation for the observed experimental suppression in activity of low atom % Mn. Recent literature has pointed to the importance of the Mn oxidation state, particularly the Mn^{3+} state, in water oxidation and indicates that the ability to easily change oxidation states is important in catalytic activity toward OER.[46−48] ALD MnO is known to oxidize under OER conditions to an average oxidation state of 3.3−3.7 depending on testing conditions.[49] From the high-resolution XPS scans of Ti and Mn (Figure 2), it is apparent that the alloying of these two oxides affects the electronic states of the atoms, and films with a greater amount of Ti begin with a slightly higher initial oxidation state of the Mn. It is possible that the Ti affects the ability of the Mn to reach the most active state, altering the way the Mn switches oxidation states, consequently resulting in lower activity of the film. Another possibility is that the mechanism associated with the lowest overpotential requires two or more Mn centers in close proximity. Thus, the degree of mixing is an important variable to control for in the design of catalysts, even for systems in which electrocatalysts are combined with a relatively

DOI: 10.1021/cs501532b
ACS Catal. 2015, 5, 1609−1616

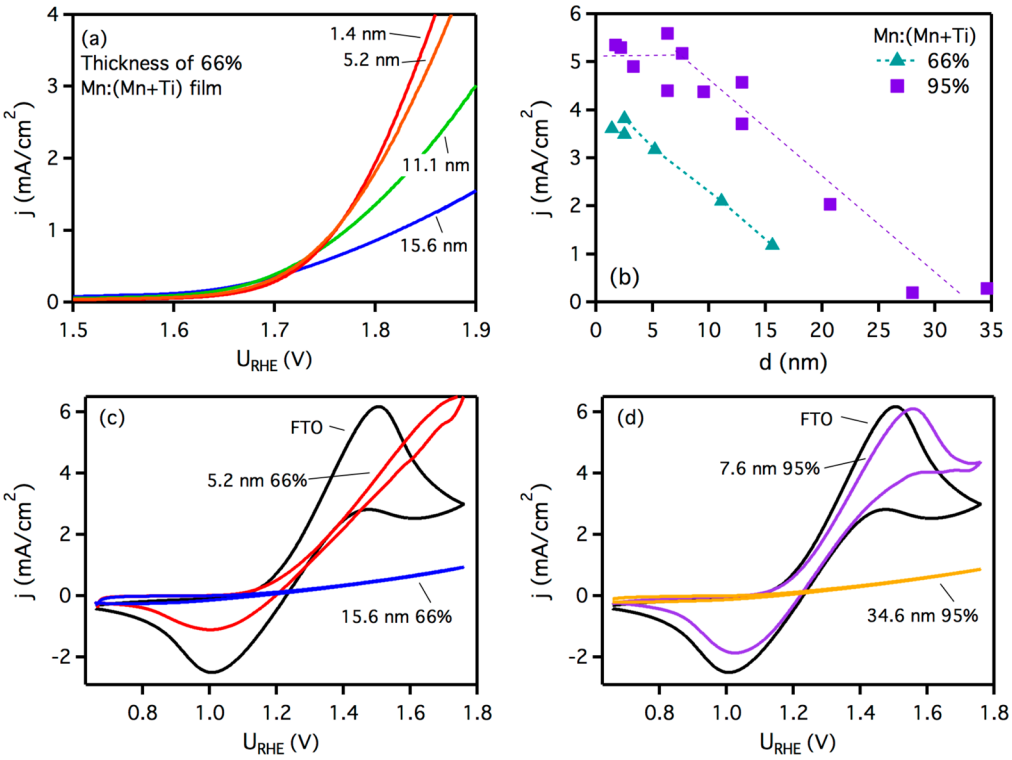

Figure 4. The importance of using thin films is highlighted by making samples of different thicknesses and testing their catalytic activity. (a) CVs for 66% Mn:(Mn+Ti) (XPS) reveal decreasing activity with increasing thickness. (b) Samples of different thicknesses displaying this trend, as evidenced by the current density at 1.85 V for 66% Mn:(Mn+Ti) and 95% Mn:(Mn+Ti) versus thickness. The deleterious effect of film thickness is believed to be due to charge transport. Lines are given to guide the eye. Probe of the charge transport using a $Fe(CN)_6^{2+/3+}$ redox couple for (c) 66% Mn:(Mn+Ti) and (d) 95% Mn:(Mn+Ti) (XPS) Mn. The current decreases with increasing film thickness, confirming that the reduced activity is related to charge transport limitations.

inert substrate such as TiO_2. For example, in the PEC splitting of water, TiO_2 has played a foundational role and hence there is interest in applying thin layers of catalysts on TiO_2 by ALD.[22,50] Small amounts of MnO_x can greatly enhance the activity of TiO_2, and MnO_x has been previously used to improve the activity of TiO_2 nanowire photoanodes.[51] However, as shown by the current results, for the highest activity, less thoroughly mixed Ti−Mn oxides may be preferred. Other material systems may also demonstrate similar properties.

The use of a thin film platform allows for study of the thickness dependence of the electrocatalyst.[10,11] In thicker films, charge transport can become rate limiting, masking the catalytic activity of the surface. We have recently shown that for thin films of ALD-TiO_2 deposited under conditions similar to those in this paper, charge transport limitations mask the catalytic activity by $d_{exptl} \approx 4$ nm.[14] By comparison, ALD-MnO_x of ∼44 nm in thickness retained high catalytic activity.[24] Guided by these earlier results, we grew all samples used for comparison of catalytic activity than 3 nm to help reduce any effects of charge transport in the catalytic testing of the films. However, by changing the thickness of the Mn−Ti oxide films systematically, we can investigate the thickness-dependent transport in these mixed metal oxide materials.

The effect of film thickness on the catalytic activity of the films was explored for films containing two different Mn concentrations: 66 and 95 atom %. Both compositions display a drop in activity beyond a critical thickness. The anodic direction of the first CV for a film containing the 66 atom % Mn:(Mn+Ti) sample is shown in Figure 4a, and the current densities at 1.85 V_{RHE} versus thickness for films containing both the 95 and 66 atom % Mn:(Mn+Ti) films are plotted in Figure 4b. For the thinnest films, the activity of the 66% Mn:(Mn+Ti) sample is lower than that of the 95 atom % Mn:(Mn+Ti) film, as expected from the discussion above. Moreover, the activities of the 66 atom % Mn:(Mn+Ti) samples begin to decrease beyond ∼5 nm. The 95 atom % Mn:(Mn+Ti) samples appear to retain their activity at greater thicknesses than do the 66 atom % Mn:(Mn+Ti) samples, but eventually the activity of the 95 atom % Mn:(Mn+Ti) film also decays, once a critical thickness of ∼10 nm is surpassed. This behavior is consistent with a model in which charge transport becomes limiting beyond critical film thickness, as described in systems of TiO_2.[14] Initially the current stays approximately constant with increasing thickness, likely because the subsurface sites are inaccessible to the electrolyte. The inaccessibility of the Mn can be further emphasized by plotting current density per mass loading of Mn (Figure S3 in the Supporting Information), where a decay in the activity of a mass loading basis is seen with increasing film thickness. This decay is even more dramatic for films beyond the critical charge transport thickness because of a combination of both a lower proportion of electrochemically accessible Mn in the film and charge transport limitations. When the charge transport cannot supply an adequate number of holes to the active sites, some voltage is lost to polarize the film, causing a decrease in the activity.

To confirm that the reduction in catalytic activity is related to charge transport limitations and not to a change in the surface chemistry of the electrocatalyst with thickness, we also probed the conductivity of the film using a $Fe(CN)_6^{3+/4+}$ redox couple.

DOI: 10.1021/cs501532b
ACS Catal. 2015, 5, 1609−1616

This redox couple undergoes an outer-sphere redox reaction; thus, it is relatively insensitive to the chemistry of the surface.[52−54] Instead, it directly probes the conductivity of the film. The redox couple and pH of the solution are selected to investigate similar conditions occurring under OER conditions, placing the redox potential at ∼1.25 V. Representative CVs for bare FTO, 5.2 nm containing 66 atom % Mn:(Mn+Ti) and 15.6 nm containing 66 atom % Mn:(Mn+Ti), are shown in Figure 4c. On bare FTO, both an oxidation and reduction feature are observed. Upon addition of 5.2 nm of Ti−Mn oxide film with 66% Mn:(Mn+Ti) composition, the distance between the peaks broadens, indicative of a greater difficulty in the redox reactions of $Fe(CN)_6^{3+/4+}$ due to charge transport limitations. With the addition of 15.6 nm of film, no distinct maxima in the redox features are discernible over the range of voltages tested, indicating large barriers to charge transport. This result is consistent with OER measurements, where the low activity is seen for the thicker films. A similar trend is observed for films containing 95 atom % Mn:(Mn+Ti), in Figure 4d. Hence, this work shows that mixed Mn−Ti oxide films suffer from charge transport limitations at thicknesses as small as 4−10 nm at compositions when the Mn content decreases below 95 atom % Mn:(Mn+Ti), further motivating the use of a technique such as ALD to fabricate ultrathin catalysts.

IV. CONCLUSIONS

Ternary oxides are promising material candidates for OER catalysts, although control over the synthesis and surface composition can prove difficult. In this study, we used ALD to deposit mixtures of Mn and Ti oxides, two oxide materials of high interest to the field of catalysis. We have characterized the deposition of these thin films and shown that good mixing occurs between the two oxides. The catalytic activity for OER was investigated by CV, and it is observed that the activity decreases with increasing Ti concentration. Interestingly, it appears that the Ti alters the electronic state of the active Mn sites, reducing their activity. While this is indicative of the good mixing achievable by ALD, different material combinations must be explored to achieve better activity. The importance of using thin films is also emphasized by showing the impact of charge transport, which can become rate limiting. For some compositions, the critical thickness at which charge transport dominates is less than ∼5 nm. This is the first study of ternary oxide electrocatalysts created by ALD, and the results indicate that it is an excellent method to explore mixtures of different oxides. This technique has the added benefit of being easily translated to coating high-surface-area, nanostructured supports for advanced catalytic design.

■ ASSOCIATED CONTENT

Supporting Information

The following file is available free of charge on the ACS Publications website at DOI: 10.1021/cs501532b.

Information on the stability of the catalysts and CVs plotted as current per mass of active catalyst (PDF)

■ AUTHOR INFORMATION

Corresponding Author

*E-mail for S.F.B.: sbent@stanford.edu.

Notes

The authors declare no competing financial interest.

■ ACKNOWLEDGMENTS

This work was supported as part of the Center on Nanostructuring for Efficient Energy Conversion (CNEEC), an Energy Frontier Research Center funded by the U.S. Department of Energy, Office of Science, Basic Energy Sciences, under Award No. DE-SC0001060. K.L.P. acknowledges a graduate fellowship through the NSF. The authors thank Aleksandra Vojvodic for useful discussions.

■ REFERENCES

(1) Lewis, N. S.; Nocera, D. G. *Proc. Natl. Acad. Sci. U.S.A.* **2007**, *104*, 20142−20142.
(2) Moats, M. S. *Jom-Us* **2008**, *60*, 46−49.
(3) Surendranath, Y.; Nocera, D. G. In *Progress in Inorganic Chemistry*; Karlin, K. D., Ed.; Wiley: Hoboken, NJ, 2011; pp 505−560.
(4) Song, M.-K.; Park, S.; Alamgir, F. M.; Cho, J.; Liu, M. *Materials Science and Engineering: R: Reports* **2011**, *72*, 203−252.
(5) Park, S.; Shao, Y.; Liu, J.; Wang, Y. *Energy Environ. Sci.* **2012**, *5*, 9331−9344.
(6) Surendranath, Y.; Bediako, D. K.; Nocera, D. G. *Proc. Natl. Acad. Sci. U.S.A.* **2012**, *109*, 15617−15621.
(7) Walter, M. G.; Warren, E. L.; McKone, J. R.; Boettcher, S. W.; Mi, Q. X.; Santori, E. A.; Lewis, N. S. *Chem. Rev.* **2010**, *110*, 6446−6473.
(8) Yeo, B. S.; Bell, A. T. *J. Am. Chem. Soc.* **2011**, *133*, 5587−5593.
(9) Gorlin, Y.; Jaramillo, T. F. *J. Am. Chem. Soc.* **2010**, *132*, 13612−13614.
(10) Trasatti, S. *Electrochim. Acta* **1991**, *36*, 225−241.
(11) Trotochaud, L.; Ranney, J. K.; Williams, K. N.; Boettcher, S. W. *J. Am. Chem. Soc.* **2012**, *134*, 17253−17261.
(12) Cheng, F.; Shen, J.; Peng, B.; Pan, Y.; Tao, Z.; Chen, J. *Nat. Chem.* **2011**, *3*, 79−84.
(13) Bediako, D. K.; Surendranath, Y.; Nocera, D. G. *J. Am. Chem. Soc.* **2013**, *135*, 3662−3674.
(14) Viswanathan, V.; Pickrahn, K.; Luntz, A. C.; Bent, S. F.; Norskov, J. K. *Nano Lett.* **2014**, *14*, 5853−5857.
(15) Singh, R. N.; Hamdani, M.; Koenig, J. F.; Poillerat, G.; Gautier, J. L.; Chartier, P. *J. Appl. Electrochem.* **1990**, *20*, 442−446.
(16) Trotochaud, L.; Boettcher, S. W. *Scripta Materialia* **2014**, *74*, 25−32.
(17) O'Hayre, R. P.; Cha, S.-W.; Colella, W.; Prinz, F. B. *Fuel Cell Fundamentals*; Wiley: Hoboken, NJ, 2006.
(18) George, S. M. *Chem. Rev.* **2010**, *110*, 111−131.
(19) Peng, Q.; Lewis, J. S.; Hoertz, P. G.; Glass, J. T.; Parsons, G. N. *J. Vac. Sci. Technol. A* **2012**, *30*, 010803.
(20) Ponraj, J. S.; Attolini, G.; Bosi, M. *Crit. Rev. Solid State* **2013**, *38*, 203−233.
(21) Jiang, X. R.; Gur, T. M.; Prinz, F. B.; Bent, S. F. *Chem. Mater.* **2010**, *22*, 3024−3032.
(22) Chen, Y. W.; Prange, J. D.; Duhnen, S.; Park, Y.; Gunji, M.; Chidsey, C. E. D.; McIntyre, P. C. *Nat. Mater.* **2011**, *10*, 539−544.
(23) Feng, H.; Lu, J. L.; Stair, P. C.; Elam, J. W. *Catal. Lett.* **2011**, *141*, 512−517.
(24) Pickrahn, K. L.; Park, S. W.; Gorlin, Y.; Lee, H. B. R.; Jaramillo, T. F.; Bent, S. F. *Adv. Energy Mater.* **2012**, *2*, 1269−1277.
(25) Feng, H.; Elam, J. W.; Libera, J. A.; Pellin, M. J.; Stair, P. C. *J. Catal.* **2010**, *269*, 421−431.
(26) Riha, S. C.; Klahr, B. M.; Tyo, E. C.; Seifert, S.; Vajda, S.; Pellin, M. J.; Hamann, T. W.; Martinson, A. B. F. *ACS Nano* **2013**, *7*, 2396−2405.
(27) Holme, T. P.; Lee, C.; Prinz, F. B. *Solid State Ionics* **2008**, *179*, 1540−1544.
(28) Elam, J. W.; George, S. M. *Chem. Mater.* **2003**, *15*, 1020−1028.
(29) Tanskanen, J. T.; Hägglund, C.; Bent, S. F. *Chem. Mater.* **2014**, *26*, 2795−2802.
(30) Ageh, V. a.; M, H.; Scharf, T. W. *Surf. Coat. Technol.* **2014**, *241*, 112−117.
(31) Jogi, I.; Tamm, A.; Kukli, K.; Kemell, M.; Lu, J.; Sajavaara, T.; Ritala, M.; Leskela, M. *J. Electrochem. Soc.* **2010**, *157*, G202−G210.

DOI: 10.1021/cs501532b
ACS Catal. 2015, 5, 1609−1616

(32) Kong, B. H.; Choi, M. K.; Cho, H. K.; Kim, J. H.; Baek, S.; Lee, J. H. *Electrochem Solid St* **2010**, *13*, K12−K14.
(33) Bakke, J. R.; Pickrahn, K. L.; Brennan, T. P.; Bent, S. F. *Nanoscale* **2011**, *3*, 3482−3508.
(34) Hultqvist, A.; Edoff, M.; Torndahl, T. *Prog. Photovoltaics* **2011**, *19*, 478−481.
(35) Man, I. C.; Su, H. Y.; Calle-Vallejo, F.; Hansen, H. A.; Martinez, J. I.; Inoglu, N. G.; Kitchin, J.; Jaramillo, T. F.; Norskov, J. K.; Rossmeisl, J. *ChemCatChem* **2011**, *3*, 1159−1165.
(36) Guo, L.; Li, X.; Chen, G. In *Electrochemistry for the Environment*; Comninellis, C., Chen, G., Eds.; Springer: New York, 2010; pp 55−98.
(37) Greeley, J.; Stephens, I. E. L.; Bondarenko, A. S.; Johansson, T. P.; Hansen, H. A.; Jaramillo, T. F.; Rossmeisl, J.; Chorkendorff, I.; Norskov, J. K. *Nat. Chem.* **2009**, *1*, 552−556.
(38) Norskov, J. K.; Bligaard, T.; Rossmeisl, J.; Christensen, C. H. *Nat. Chem.* **2009**, *1*, 37−46.
(39) Morales, M. R.; Barbero, B. P.; Cadus, L. E. *Appl. Catal. B-Environ.* **2007**, *74*, 1−10.
(40) Garcia-Mota, M.; Vojvodic, A.; Metiu, H.; Man, I. C.; Su, H. Y.; Rossmeisl, J.; Norskov, J. K. *ChemCatChem.* **2011**, *3*, 1607−1611.
(41) Burton, B. B.; Fabreguette, F. H.; George, S. M. *Thin Solid Films* **2009**, *517*, 5658−5665.
(42) Xie, Q.; Jiang, Y. L.; Detavernier, C.; Deduytsche, D.; Van Meirhaeghe, R. L.; Ru, G. P.; Li, B. Z.; Qu, X. P. *J. Appl. Phys.* **2007**, *102*, 083521.
(43) Ritala, M.; Leskela, M.; Niinisto, L.; Haussalo, P. *Chem. Mater.* **1993**, *5*, 1174−1181.
(44) Gong, M. C.; Zhou, J. L.; Xu, Z. H.; Chen, Y. Q.; Chen, Y. *Catal. Today* **1995**, *24*, 259−261.
(45) Liu, F. M.; Wang, T. M.; Li, J. Q.; Wang, C.; Zheng, S. K.; Duan, M. *J. Magn. Magn. Mater.* **2002**, *251*, 245−250.
(46) Hocking, R. K.; Brimblecombe, R.; Chang, L. Y.; Singh, A.; Cheah, M. H.; Glover, C.; Casey, W. H.; Spiccia, L. *Nat. Chem.* **2011**, *3*, 461−466.
(47) Jiao, F.; Frei, H. *Chem. Commun.* **2010**, *46*, 2920−2922.
(48) Takashima, T.; Hashimoto, K.; Nakamura, R. *J. Am. Chem. Soc.* **2012**, *134*, 1519−1527.
(49) Pickrahn, K. L.; Gorlin, Y.; Seitz, L. C.; Garg, A.; Nordlund, D.; Jaramillo, T. F.; Bent, S. F. Manuscript in preparation.
(50) Hu, S.; Shaner, M. R.; Beardslee, J. A.; Lichterman, M.; Brunschwig, B. S.; Lewis, N. S. *Science* **2014**, *344*, 1005−1009.
(51) Resasco, J.; Dasgupta, N. P.; Rosell, J. R.; Guo, J.; Yang, P. *J. Am. Chem. Soc.* **2014**, *136*, 10521−10526.
(52) Heusler, K. E.; Yun, K. S. *Electrochim. Acta* **1977**, *22*, 977−986.
(53) Macpherson, J. V.; de Mussy, J. P. G.; Delplancke, J. L. *J. Electrochem. Soc.* **2002**, *149*, B306−B313.
(54) Stoerzinger, K. A.; Risch, M.; Suntivich, J.; Lu, W. M.; Zhou, J.; Biegalski, M. D.; Christen, H. M.; Ariando; Venkatesan, T.; Shao-Horn, Y. *Energy Environ. Sci.* **2013**, *6*, 1582−1588.

DOI: 10.1021/cs501532b
ACS Catal. 2015, 5, 1609−1616